Lysophosphatidylinositol-induced activation of the cation channel TRPV2 triggers glucagon-like peptide-1 secretion in enteroendocrine L cells

Received for publication, March 28, 2017, and in revised form, May 17, 2017 Published, Papers in Press, May 22, 2017, DOI 10.1074/jbc.M117.788653

Kazuki Harada[‡], Tetsuya Kitaguchi[§¶], Taichi Kamiya[‡], Kyaw Htet Aung[‖], Kazuaki Nakamura[‖], Kunihiro Ohta[‡], and Takashi Tsuboi[‡1]

From the [‡]Department of Life Sciences, Graduate School of Arts and Sciences, The University of Tokyo, Tokyo 153-8902, Japan, [§]Cell Signaling Group, Waseda Bioscience Research Institute in Singapore (WABIOS), Singapore 138667, Singapore, [¶]Comprehensive Research Organization, Waseda University, Tokyo 162-0041, Japan, and [‖]National Research Institute for Child Health and Development, Tokyo 157-8535, Japan

Edited by Henrik G. Dohlman

The lysophosphatidylinositol (LPI) has crucial roles in multiple physiological processes, including insulin exocytosis from pancreatic islets. However, the role of LPI in secretion of glucagon-like peptide-1 (GLP-1), a hormone that enhances glucose-induced insulin secretion, is unclear. Here, we used the murine enteroendocrine L cell line GLUTag and primary murine small intestinal cells to elucidate the mechanism of LPI-induced GLP-1 secretion. Exogenous LPI addition increased intracellular Ca^{2+} concentrations ($[Ca^{2+}]_i$) in GLUTag cells and induced GLP-1 secretion from both GLUTag and acutely prepared primary intestinal cells. The $[Ca^{2+}]_i$ increase was suppressed by an antagonist for G protein-coupled receptor 55 (GPR55) and by silencing of GPR55 expression, indicating involvement of G_q and $G_{12/13}$ signaling pathways in the LPI-induced increased $[Ca^{2+}]_i$ levels and GLP-1 secretion. However, GPR55 agonists did not mimic many of the effects of LPI. We also found that phospholipase C inhibitor and Rho-associated kinase inhibitor suppressed the $[Ca^{2+}]_i$ increase and that LPI increased the number of focal adhesions, indicating actin reorganization. Of note, blockage or silencing of transient receptor potential cation channel subfamily V member 2 (TRPV2) channels suppressed both the LPI-induced $[Ca^{2+}]_i$ increase and GLP-1 secretion. Furthermore, LPI accelerated TRPV2 translocation to the plasma membrane, which was significantly suppressed by a GPR55 antagonist. These findings suggest that TRPV2 activation via actin reorganization induced by G_q and $G_{12/13}$ signaling is involved in LPI-stimulated GLP-1 secretion in enteroendocrine L cells. Because GPR55 agonists largely failed to mimic the effects of LPI, its actions on L cells are at least partially independent of GPR55 activation.

This work was supported in part by Grants-in-aid for Scientific Research (26460289 (to T. T.) and 26291018 (to K. O.) from the Ministry of Education, Culture, Sports, Science, and Technology of Japan. The authors declare that they have no conflicts of interest with the contents of this article.

This article contains supplemental Movie 1 and Figs. 1 and 2.

[1] To whom correspondence should be addressed: Dept. of Life Sciences, Graduate School of Arts and Sciences, University of Tokyo, 3-8-1 Komaba, Meguro, Tokyo 153-8902, Japan. Tel./Fax: 81-3-5465-8208; E-mail: takatsuboi@bio.c.u-tokyo.ac.jp.

Stimulus-coupled secretion of glucagon-like peptide-1 (GLP-1)[2] from enteroendocrine L cells plays a fundamental role in glucose homeostasis, as secreted GLP-1 enhances glucose-induced insulin secretion from pancreatic β cells (1–3). Drugs that artificially improve the effect of GLP-1, such as GLP-1 analogues or inhibitors of GLP-1 degrading enzymes, are used in clinical treatment. Understanding the precise molecular mechanism underlying endogenous GLP-1 secretion will provide further insight for the treatment of type 2 diabetes. Recent studies have revealed stimulatory effects of luminal nutrients including glucose, amino acids, and fatty acids on GLP-1 secretion from the L cells (4–7). In contrast, the involvement of circulating metabolism-related molecules, such as stress hormones and inflammatory cytokines, are still partially clarified (8–10).

Lysophospholipids are phospholipids with only one long fatty acid chain produced by phospholipase A (11). They are not only components of the plasma membrane but also act as bioactive lipid messengers to regulate a variety of physiological processes, including immunity, tumorigenesis, and nociception (12). Among these is lysophosphatidylinositol (LPI), which was suggested almost 30 years ago to play a Ca^{2+}-dependent potentiating role in insulin exocytosis from pancreatic islets (13, 14). Although studies have been performed on the contribution of LPI to membrane potential regulation (15–17), cell migration (16), and endothelial relaxation (18), little has been explored regarding the effect of LPI on hormone secretion (15, 19). This is in part because the specific receptor and downstream signaling pathways for LPI have not been identified.

An orphan G protein-coupled receptor 55 (GPR55) was identified as a specific LPI receptor (20, 21). Subsequent studies were performed to clarify the intracellular signal cascades downstream of GPR55, mainly with GPR55-overexpressing HEK293 cells (20, 22–24) or the human endothelial cell line EA.hy926, which endogenously expresses GPR55 (25, 26).

[2] The abbreviations used are: GLP-1, glucagon-like peptide-1; Fsk, forskolin; IBMX, 3-isobutyl 1-methylxanthine; LPI, lysophosphatidylinositol; GPR55, G protein-coupled receptor 55; TRPV2, transient receptor potential cation channel subfamily V member 2; TIRF, total internal reflection fluorescence; PLC, phospholipase C; ROCK, Rho-associated kinase; RR, ruthenium red; RB, Ringer Buffer; ANOVA, analysis of variance.

Although GPR55 is generally coupled to either G_q or $G_{12/13}$ proteins, experiments with HEK293 cells showed the activation of cAMP response element-binding protein (CREB), extracellular signal-regulated kinase (ERK), and nuclear factor-κB (NFκB) signaling pathways (23), and those with EA.hy926 cells demonstrated the involvement of phosphatidylinositol 3-kinase (PI3K), integrin, and intermediate-conductance Ca^{2+}-activated K^+ channels (25, 26).

Recent studies have shown that pancreatic islets express GPR55, and the application of GPR55 agonist enhanced the glucose-stimulated increase in intracellular Ca^{2+} concentration ($[Ca^{2+}]_i$), clarifying a potential mechanism of LPI-induced insulin secretion (13, 14, 27, 28). Moreover, the expression level of GPR55 in adipose tissues and the circulating LPI concentration were increased in obese human subjects (29), and the circulating level of LPI is reduced during fasting (30). These results suggest the involvement of LPI and GPR55 in glucose homeostasis. However, neither the role of LPI on the release of GLP-1 or the specific molecular mechanisms of LPI-induced hormone secretion from enteroendocrine L cells are largely unknown.

In this study we used the enteroendocrine L cell line GLUTag to elucidate the molecular mechanisms of LPI-induced GLP-1 secretion. We found that GLUTag cells endogenously express GPR55. Application of LPI induced a significant increase in $[Ca^{2+}]_i$ and GLP-1 secretion. GLP-1 secretion was also enhanced by LPI in primary intestinal cells from mice. Inhibition of GPR55 by an antagonist, silencing of GPR55 by a small interfering RNA (siRNA), and inhibition of the G_q and $G_{12/13}$ pathways by a phospholipase C (PLC) inhibitor and a Rho-associated kinase (ROCK) inhibitor suppressed the LPI-induced $[Ca^{2+}]_i$ increase. Furthermore, blockage and silencing of transient potential receptor cation channel subfamily V member 2 (TRPV2) also suppressed the LPI-induced $[Ca^{2+}]_i$ increase and GLP-1 secretion. Interestingly, application of LPI to the cells induced the translocation of TRPV2 to the plasma membrane revealed by total internal reflection fluorescence microscopy. These results suggest that LPI induces GLP-1 secretion from enteroendocrine L cells through the activation of the GPR55, ROCK, and TRPV2 pathways.

Results

LPI increased $[Ca^{2+}]_i$ in GLUTag cells via GPR55

To examine the effect of LPI on GLP-1 secretion from enteroendocrine L cells, we first monitored intracellular Ca^{2+} dynamics using the Ca^{2+}-sensing dye Fluo-4 AM in GLUTag cells. Application of LPI induced an $[Ca^{2+}]_i$ increase with prolonged oscillatory responses, and the area under curve of fluorescence intensity of Fluo-4 was significantly increased (Fig. 1, *A* and *B*). 2 μM LPI was sufficient to significantly enhance GLP-1 secretion as determined by ELISA (Fig. 1*C*). Furthermore, application of 10 μM LPI significantly increased GLP-1 secretion in primary mouse small intestinal cells (Fig. 1*D*).

To clarify the signaling cascades involved in the LPI-induced $[Ca^{2+}]_i$ increase, we examined the contribution of GPR55, an LPI receptor. As determined by RT-PCR, GPR55 was expressed in GLUTag cells (Fig. 2*A* and supplemental Fig. S1*A*). Co-application of the GPR55 antagonist O-1918 with LPI significantly

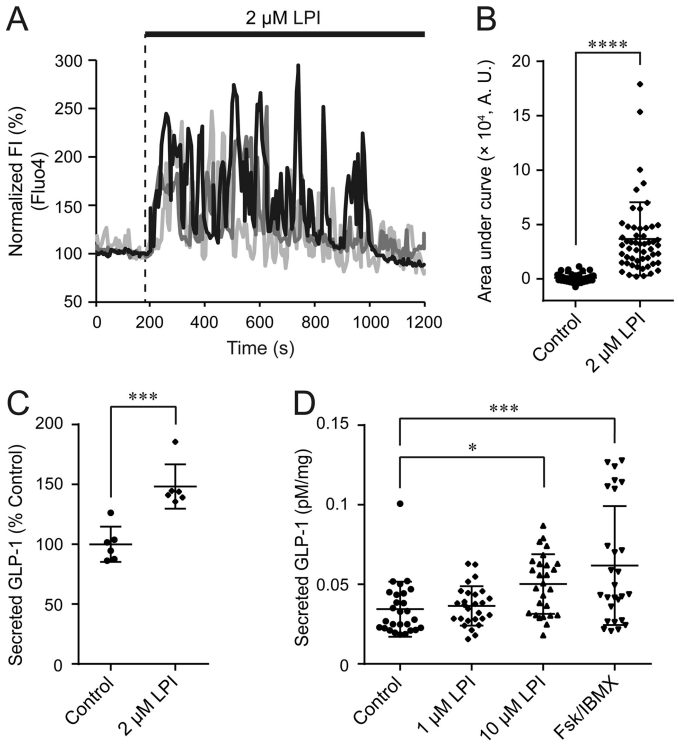

Figure 1. LPI induced $[Ca^{2+}]_i$ increase and GLP-1 secretion in GLUTag cells and primary cultured mouse small intestinal cells. *A*, typical time courses of $[Ca^{2+}]_i$ during the application of 2 μM LPI to GLUTag cells. *FI*, fluorescence intensity. *B*, area under the curve calculated from the fluorescence intensity of Fluo-4 by the application of LPI; Welch's *t* test. $n \geq 37$ cells. *C*, the amount of secreted GLP-1 in GLUTag cells after the application of 2 μM LPI. Data are one-way ANOVA with Tukey's post hoc test (with Fig. 4*D*). $n = 6$ experiments. *D*, amount of secreted GLP-1 in primary cultured mouse small intestinal cells after the application of 1 μM LPI, 10 μM LPI, or 10 μM Fsk + 100 μM IBMX. Data are one-way ANOVA with Tukey's post hoc test. $n = 27$ experiments from 9 mice. Data are shown as the mean ± S.D. *, $p < 0.5$; ***, $p < 0.001$; ****, $p < 0.0001$.

reduced the LPI-induced $[Ca^{2+}]_i$ increase (Fig. 2, *B* and *C*). Silencing of endogenous GPR55 expression using a specific siRNA also significantly suppressed the LPI-induced $[Ca^{2+}]_i$ increase (Fig. 2, *D* and *E*, and supplemental Fig. S1*B*). These results suggest that GPR55 functions as a receptor through which LPI induces $[Ca^{2+}]_i$ increase in enteroendocrine L cells.

LPI induced $[Ca^{2+}]_i$ increase and actin reorganization through the G_q and $G_{12/13}$ pathways

Because GPR55 is generally coupled to G_q or $G_{12/13}$ proteins, we next examined the effect of the PLC inhibitor U-73122 and the ROCK inhibitor Y-27632 to clarify the involvement of these pathways downstream of GPR55. Co-application of either U-73122 or Y-27632 with LPI significantly suppressed the LPI-induced $[Ca^{2+}]_i$ increase (Fig. 3, *A*–*D*). These results suggest that both PLC- and RhoA-mediated signals are involved in the LPI-induced $[Ca^{2+}]_i$ increase. Although we also examined the involvement of PI3K pathway using a PI3K inhibitor LY294002, co-application of LY294002 with LPI had little effect (Fig. 3, *E* and *F*).

To investigate the role of RhoA-mediated signals in response to LPI, we analyzed subplasma membrane actin dynamics by total internal reflection fluorescence (TIRF) microscopy using the actin visualizing fluorescent protein Lifeact-EGFP

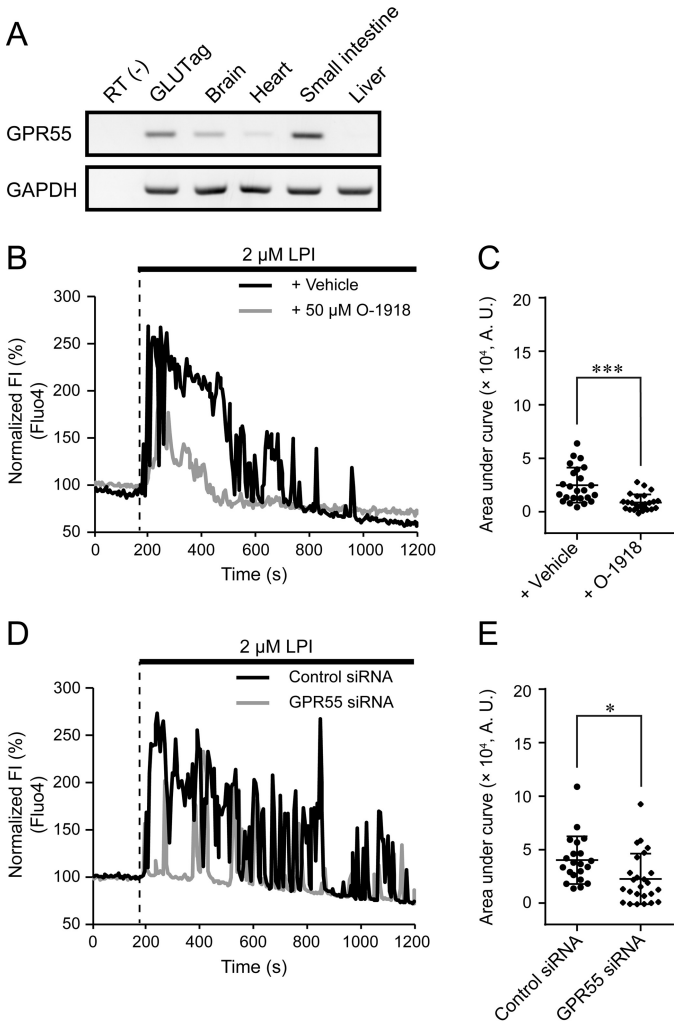

Figure 2. Involvement of GPR55 in LPI-induced $[Ca^{2+}]_i$ increase. *A*, RT-PCR analysis for GPR55 in GLUTag cells. $n = 3$ experiments. *B*, typical time courses of $[Ca^{2+}]_i$ during the co-application of 50 μM O-1918 with 2 μM LPI. *FI*, fluorescence intensity. *C*, area under the curve calculated from the fluorescence intensity of Fluo-4 by the co-application of O-1918 with LPI; Welch's *t* test. $n \geq 24$ cells. *A.U.*, absorbance units. *D*, typical time courses of $[Ca^{2+}]_i$ during the application of 2 μM LPI in GPR55-depleted GLUTag cells. *E*, area under the curve calculated from the fluorescence intensity of Fluo-4 by the application of LPI in GPR55-depleted GLUTag cells; Welch's *t* test. $n \geq 29$ cells. Data are shown as the mean ± S.D. *, $p < 0.05$; ***, $p < 0.001$.

(31). After the application of LPI, Lifeact-EGFP fluorescent fibers became thicker in the leading edge of the plasma membrane (Fig. 3*G*). Additionally, we found a significant increase in punctate fluorescent signals throughout the subplasma membrane. These signals were likely focal adhesions formed by RhoA GTPase (32, 33) (Fig. 3*G*, *insets*, and *H*). These results suggest that actin reorganization contributes to LPI-induced GLP-1 secretion through the G_q and $G_{12/13}$ pathways.

TRPV2 was involved in LPI-induced $[Ca^{2+}]_i$ increase and GLP-1 secretion

We explored additional signaling pathways that could contribute to $[Ca^{2+}]_i$ increase. LPI induces $[Ca^{2+}]_i$ increase in TRPV2-overexpressing HEK293 cells (16); therefore, we examined the involvement of TRPV2 in LPI-induced $[Ca^{2+}]_i$ increase in GLUTag cells. We confirmed expression of TRPV2 mRNA in GLUTag cells by RT-PCR (Fig. 4*A* and supplemental Fig. S1*C*). Co-application of the TRP channel blocker ruthenium red (RR) with LPI significantly suppressed the LPI-induced $[Ca^{2+}]_i$ increase and GLP-1 secretion (Fig. 4, *B–D*). Ruthenium red used to inhibit TRPV2 activity in this study also inhibits many additional subtypes of TRP channels and is not specific for TRPV2 (34). Therefore, we next specifically silenced TRPV2 expression by siRNA. This treatment also significantly suppressed LPI-induced $[Ca^{2+}]_i$ increase and GLP-1 secretion (Fig. 4, *E–G*, and supplemental Fig. S1*D*).

To understand the mechanism of TRPV2 activation underlying the $[Ca^{2+}]_i$ increase, we monitored the localization of TRPV2 on the plasma membrane using TIRF microscopy. Application of LPI induced a gradual increase in the fluorescence intensity of TRPV2-EGFP throughout the entire plasma membrane (Fig. 5, *A* and *B*, and supplemental Movie S1). The increase in the fluorescence intensity of TRPV2-EGFP was significantly suppressed by co-application of O-1918 with LPI (Fig. 5*C*). These results suggest that LPI-induced TRPV2 translocation to the plasma membrane is involved in the $[Ca^{2+}]_i$ increase and GLP-1 secretion.

LPI-induced $[Ca^{2+}]_i$ increase and TRPV2 activation is not solely dependent on GPR55

We next investigated whether selective activation of GPR55 recapitulates the LPI-induced $[Ca^{2+}]_i$ increase, TRPV2 translocation, and GLP-1 secretion. However, application of GPR55 agonist, O-1602, had little effect on $[Ca^{2+}]_i$, fluorescence intensity of TRPV2-EGFP, or GLP-1 secretion (Fig. 6). These results suggest that the $[Ca^{2+}]_i$ increase and GLP-1 secretion is not evoked by simply activating GPR55.

Discussion

The focus of our research was to explore whether LPI induces GLP-1 secretion from enteroendocrine L cells and to clarify the precise signaling pathways downstream of LPI stimulation that contribute GLP-1 secretion. In this study we found that the enteroendocrine L cell line GLUTag exhibited a $[Ca^{2+}]_i$ increase in response to LPI via the G protein-coupled receptor GPR55 (Figs. 1 and 2). The EC_{50} of LPI estimated from Ca^{2+} imaging was 3.4 μM (supplemental Fig. 2*A*). Because the circulating level of LPI in rats is ~3 μM (30), 2 μM LPI may be sufficient to induce GLP-1 secretion from enteroendocrine L cells under physiological conditions. In the presence of 2 μM LPI, ~50–80% of observed cells showed a $[Ca^{2+}]_i$ increase (data not shown). This phenomenon may be explained by different expression levels of GPR55, TRPV2, and G_q or $G_{12/13}$ proteins.

GPR55 is involved in the G_q, $G_{12/13}$, and PI3K pathways (20, 21, 23–25). Interestingly, inhibition of PLC or ROCK significantly suppressed the $[Ca^{2+}]_i$ increase in GLUTag cells, whereas inhibition of PI3K had little effect (Fig. 3). The subfamily of heterotrimeric G proteins is heterogeneously distributed in various cells and tissues (35, 36). In contrast, many G protein-coupled receptors functionally switch the subfamily of G protein with which they are associated (37–39). Thus, these effects may be explained by the difference in expression levels and/or the functional switch between G_q and $G_{12/13}$ proteins in GLUTag cells.

Consistent with previous results (16), translocation of TRPV2 to the plasma membrane in response to LPI appears to be a key phenomenon to LPI-induced $[Ca^{2+}]_i$ increase and GLP-1 secretion (Figs. 4 and 5). Notably, inhibition or silencing of GPR55 suppressed the $[Ca^{2+}]_i$ increase (Fig. 4, *E–G*), and translocation of TRPV2 was also GPR55-dependent (Fig. 5*C*), suggesting that TRPV2 translocation takes place in response to the activation of GPR55. Because insulin-induced translocation

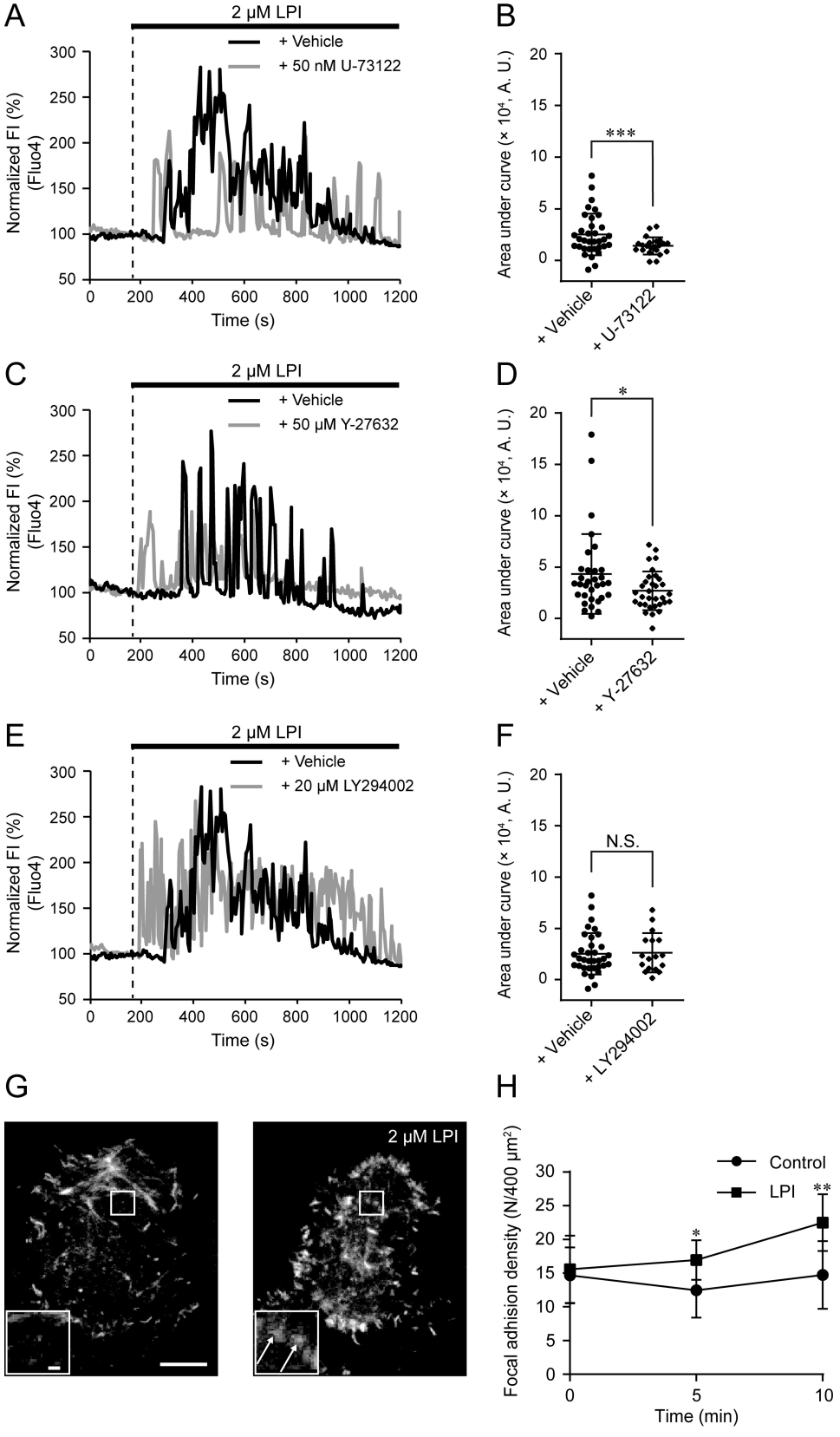

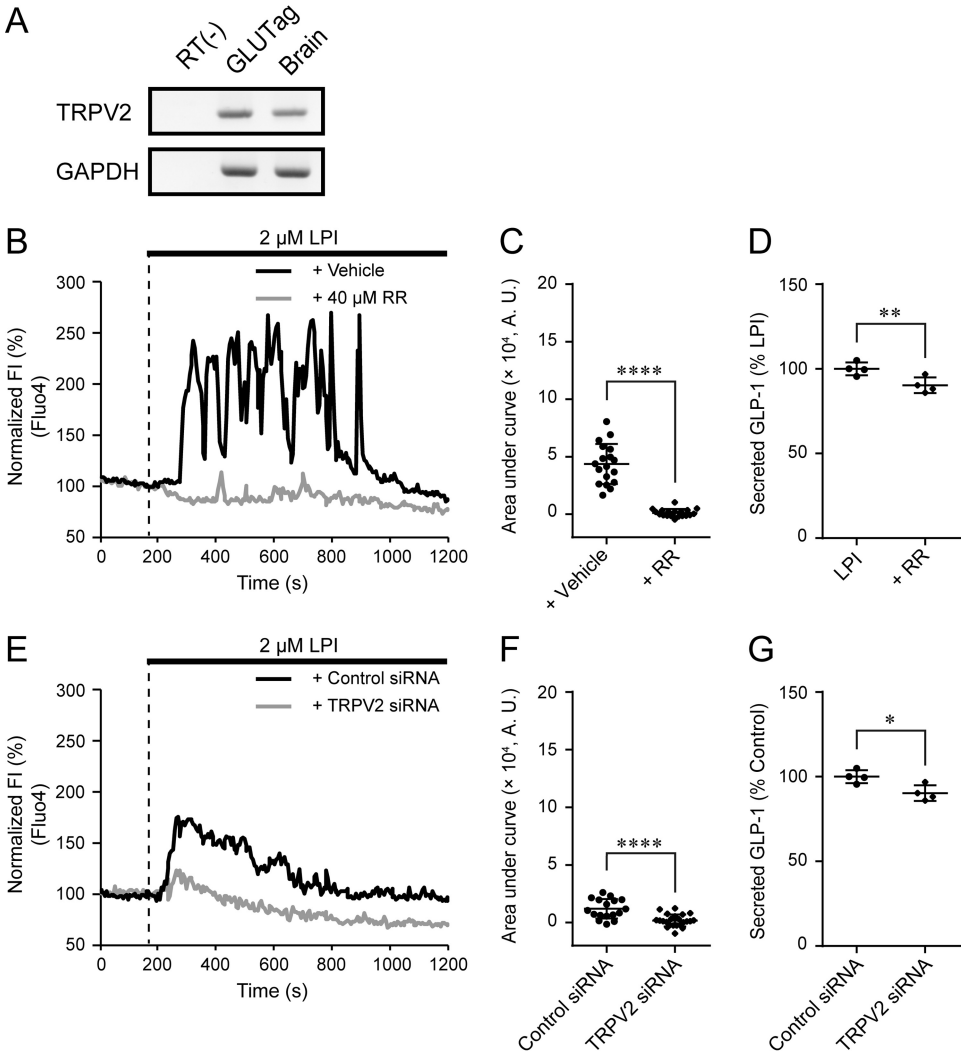

Figure 4. Involvement of TRPV2 in LPI-induced $[Ca^{2+}]_i$ increase and GLP-1 secretion. *A*, RT-PCR analysis for TRPV2 in GLUTag cells. $n = 4$ experiments. *B*, typical time courses of $[Ca^{2+}]_i$ during the co-application of 40 μM RR with 2 μM LPI. *C*, area under curve calculated from the fluorescence intensity of Fluo-4 by the co-application of RR with LPI; Welch's *t* test. $n \geq 18$ cells. *A.U.*, absorbance units. *D*, the amount of secreted GLP-1 in GLUTag cells after the co-application of RR with LPI. Data for LPI are from Fig. 1*C*. Data are one-way ANOVA with Tukey's post hoc test (with Fig. 1*C*). $n = 6$ experiments. *E*, typical time courses of $[Ca^{2+}]_i$ during the application of 2 μM LPI in TRPV2-depleted GLUTag cells. *F*, area under curve calculated from the fluorescence intensity of Fluo4 by the application of LPI in TRPV2-depleted GLUTag cells; Welch's *t* test. $n \geq 17$ cells. *G*, the amount of secreted GLP-1 in GLUTag cells after the application of LPI in TRPV2-depleted GLUTag cells. Welch's *t* test. $n = 4$ experiments. Data are shown as the mean ± S.D. *, $p < 0.05$; **, $p < 0.01$; ****, $p < 0.0001$.

of glucose transporters in adipocytes and muscle cells are RhoA- and ROCK-dependent (40–42), we speculated that translocation of TRPV2 in GLUTag cells is associated with RhoA/ROCK-dependent formation of focal adhesions. This speculation appears consistent with the previous report that TRPV2 is colocalized with proteins such as integrin, paxillin, and focal adhesion kinase (FAK) family proteins (43), which accumulate in focal adhesions.

We found that LPI increased the number of focal adhesions (Fig. 3, *G* and *H*). The increase likely contributes to increasing the number of TRPV2 channels on the plasma membrane for GLP-1 secretion in GLUTag cells. Furthermore, regulation of the actin network is an important step for vesicle trafficking (44), and coordinated assembly and disassembly of actin filaments by RhoA near the plasma membrane facilitates fusion of vesicles with the membrane (45). Therefore, facilitation of

Figure 3. PLC and ROCK-mediated $[Ca^{2+}]_i$ increase and actin reorganization in response to LPI. *A*, typical time courses of $[Ca^{2+}]_i$ during the co-application of 50 nM U-73122 with 2 μM LPI. *B*, area under curve calculated from the fluorescence intensity of Fluo-4 by the co-application of U-73122 with LPI. Data are one-way ANOVA with Dunnett's post hoc test (with Fig. 3*F*). $n \geq 22$ cells. *A.U.*, absorbance units. *C*, typical time courses of $[Ca^{2+}]_i$ during the co-application of 50 μM Y-27632 with 2 μM LPI. *D*, area under the curve calculated from the fluorescence intensity of Fluo-4 by the co-application of Y-27632 with LPI; Welch's *t* test. $n \geq 32$ cells. *E*, typical time courses of $[Ca^{2+}]_i$ during the co-application of 20 μM LY294002 with 2 μM LPI. *F*, area under the curve calculated from the fluorescence intensity of Fluo-4 by the co-application of wortmannin or LY294002 with LPI. Data for + *Vehicle* are from Fig. 3*B*. Data are one-way ANOVA with Dunnett's post hoc test (with Fig. 3*B*). $n \geq 17$ cells. *N.S.*, not significant. *G*, typical images of Lifeact-EGFP-expressing GLUTag cells before and after the application of 2 μM LPI. *Scale bar*, 10 μm. *Insets* show the enlarged images of the outlined areas. *Arrows* represent focal adhesion-like fluorescent spots. *Scale bar*, 1 μm. *H*, density of focal adhesions calculated during the application of LPI. Welch's *t* test. $n \geq 9$ cells. Data are shown as the mean ± S.D. *N.S.*, not significant; *, $p < 0.05$; **, $p < 0.01$.

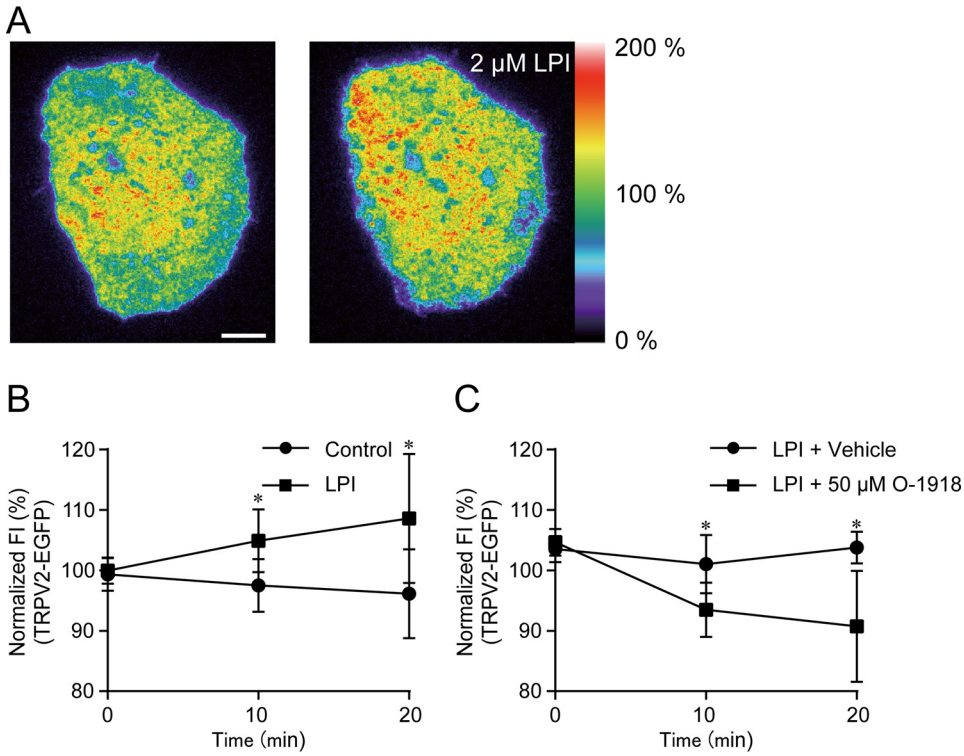

Figure 5. Translocation of TRPV2 in response to LPI. *A*, typical pseudo-color images of TRPV2-EGFP-expressing GLUTag cells during the application of 2 μM LPI. *Scale bar*, 10 μm. *B*, changes in average fluorescence intensity (*FI*) of TRPV2-EGFP-expressing GLUTag cells during the application of LPI; Welch's *t* test. $n \geq 6$ cells. *C*, changes in average fluorescence intensity of TRPV2-EGFP-expressing GLUTag cells during the co-application of 50 μM O-1918 with 2 μM LPI; Welch's *t* test. $n \geq 5$ cells. Data are shown as the mean ± S.D. *, $p < 0.05$.

fusion of TRPV2-containing vesicles also presumably contributes to enhancement of TRPV2 localization on the plasma membrane induced by LPI. Because experiments with fluorescent proteins require careful interpretation on photobleach, further study in combination with biochemical assays and electrophysiological recording will clarify the precise interplay between actin reorganization and TRPV2 translocation.

Inhibition and silencing of GPR55 partly suppressed the $[Ca^{2+}]_i$ increase and translocation of TRPV2 caused by application of LPI (Fig. 2, *B–E*), whereas blockage and silencing of TRPV2 suppressed it almost completely (Fig. 4, *B–G*). Moreover, selective activation of GPR55 did not induce the $[Ca^{2+}]_i$ increase, TRPV2 translocation, or GLP-1 secretion (Fig. 6). These results suggest the possibility that activation of TRPV2 by LPI is not solely regulated by GPR55. Interestingly, there are several TRP channels other than TRPV2 that are activated by lysophospholipids. For instance, TRPV1 is activated by direct binding of lysophosphatidic acid (46), and TRPM8 is activated by lysophosphatidylcholine and lysophosphatidylserine (47, 48). Moreover, heterologous expression of TRPV2 in HEK293 cells exhibited an $[Ca^{2+}]_i$ increase induced by LPI and lysophosphatidylcholine (16). It is conceivable that TRPV2 is also activated by direct binding of LPI. Further investigation into the biochemical interactions between TRP channels and lysophospholipids needs to be performed.

Collectively, our study showed that LPI stimulates GLP-1 secretion from both GLUTag cells and primary cultured small intestinal cells, which is mediated by both GPR55 and TRPV2 (Fig. 7). The present data clarify the precise signaling pathways provoked by LPI to induce hormone secretion and demonstrate the importance of lysophospholipid sensing for GLP-1 secretion. Although cumulative evidence reveals the relationship between LPI-GPR55 signaling and the impairment of glucose homeostasis (29, 49), we would need to examine the kinetics of circulating LPI related to food intake to clarify the interplay with GLP-1 and insulin secretion. Further research *in vivo* will provide a novel insight into therapies treating metabolic diseases including diabetes.

Experimental procedures

Chemicals

L-α-Lysophosphatidylinositol (LPI) sodium salt was purchased from Sigma. O-1918, O-1602, U-73122, and LY294002 were purchased from Cayman Chemical (Ann Arbor, MI). Forskolin (Fsk), Y-27632, and RR were purchased from WAKO Pure Chemical Industries (Osaka, Japan). 3-Isobutyl 1-methylxanthine (IBMX) was purchased from Merck.

Plasmid construction

A mouse TRPV2 clone was purchased from DNAFORM (ID 2210009M20, Kanagawa, Japan). TRPV2-EGFP was cloned by amplifying the mouse TRPV2 cDNA by PCR followed by ligation into the XhoI/EcoRI sites of pEGFP-N1. Lifeact-EGFP (kindly provided by Dr. Roland Wedlich-Soldner, Max Planck Institute of Biochemistry, Germany) was used as previously described (31).

Cell culture and plasmid transfection

GLUTag cells (kindly provided by Dr. Daniel Drucker, Lunenfeld-Tanenbaum Research Institute, Toronto, Canada)

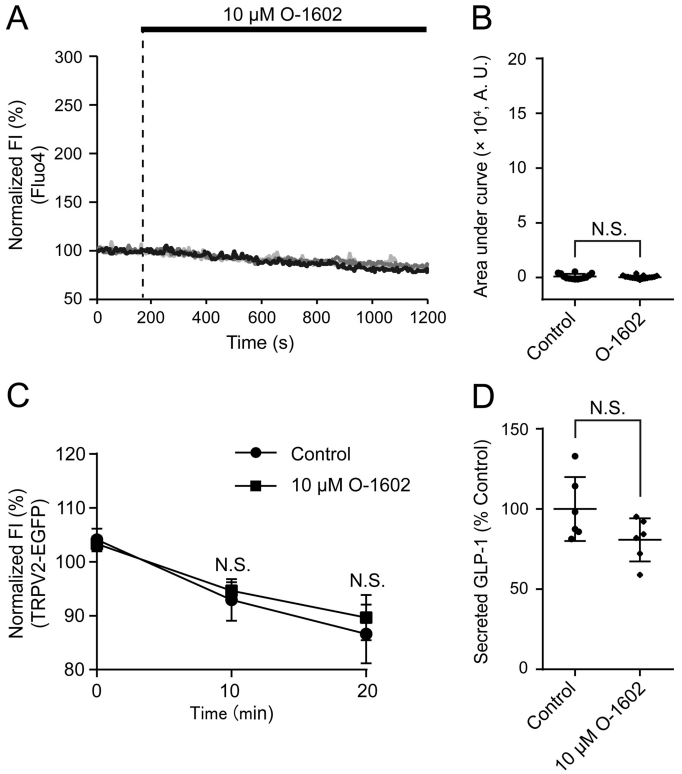

Figure 6. Effect of GPR55 activation on LPI-induced $[Ca^{2+}]_i$ increase, TRPV2 translocation, and GLP-1 secretion. *A*, typical time courses of $[Ca^{2+}]_i$ during the application of 10 μM O-1602. *B*, area under the curve calculated from the fluorescence intensity (*FI*) of Fluo-4 by the application of O-1602; Welch's *t* test. $n \geq 14$ cells. *A.U.*, absorbance units. *C*, changes in average fluorescence intensity of TRPV2-EGFP-expressing GLUTag cells during the application of O-1602. Welch's *t* test. $n = 8$ cells. *D*, the amount of secreted GLP-1 in GLUTag cells after the application of O-1602; Welch's *t* test. $n = 6$ experiments. Data are shown as the mean ± S.D. *N.S.*, not significant.

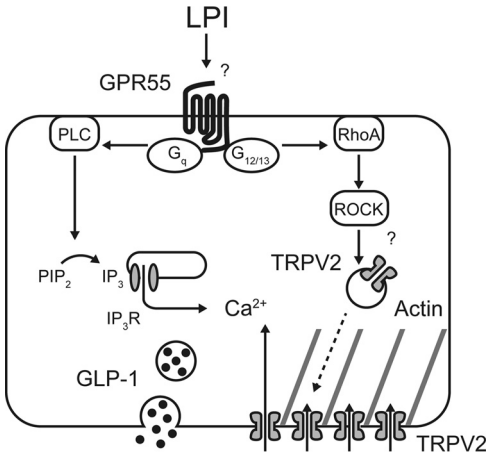

Figure 7. Schematic image of LPI-induced GLP-1 secretion from GLUTag cells. LPI binds to GPR55 and mainly activates G_q and $G_{12/13}$ proteins, which results in actin polymerization mediated by RhoA and translocation of TRPV2 to the plasma membrane. Activation of TRPV2 induces Ca^{2+} influx and promotes GLP-1 secretion.

were cultured in Dulbecco's modified Eagle's medium (Sigma) supplemented with 1 g/liter glucose, L-glutamine, sodium pyruvate, 10% (v/v) heat-inactivated fetal bovine serum (Sigma), 100 units/ml penicillin, and 100 μg/ml streptomycin (Sigma) at 37 °C under 5% CO_2. For imaging experiments, the cells were trypsinized, and 1×10^5 cells were plated onto poly-L-lysine (Sigma)-coated glass coverslips in 35-mm dishes. Two days after plating, the cells were transfected with 1.5 μg of plasmid using 3 μl of Lipofectamine 2000 Transfection Reagent (Thermo Fisher Scientific, Waltham, MA) according to the manufacturer's protocol.

RNA isolation and RT-PCR analysis

Total RNA from GLUTag cells and mouse tissues was isolated using the RNeasy Mini Kit (Qiagen, KJ Venlo, The Netherlands). After DNase treatment using RNase-Free DNase Set (Qiagen), cDNA was synthesized using the High Capacity RNA-to-cDNA kit (Thermo Fisher Scientific). Synthesized cDNA was amplified using EmeraldAmp PCR Master Mix (TaKaRa, Shiga, Japan). For PCR amplification of GPR55 (NM_001033290.2), the forward primer 5′-GACTTGGACAGCCTAGGAAGG-3′ and the reverse primer 5′-CCTTTGTGCTGCTTGGTGAAG-3′ were used. For TRPV2 (NM_011706.2), the forward primer 5′-TGTACGACCTGTCCTCTGTG-3′ and the reverse primer 5′-CAACAGCAGCATGGAGTCC-3′ were used. For glyceraldehyde-3-phosphate dehydrogenase (GAPDH, NM_001289726.1), the forward primer 5′-CCGGTGCTGAGTATGTCGTGGAGTCTAC-3′, and the reverse primer 5′-CTTTCCAGAGGGGCCATCCACAGTCTTC-3′ were used.

RNA interference of GPR55 and TRPV2

GLUTag cells plated for 24 h were transfected with 100 nM GPR55 siRNA (Silencer Select siRNA, s105617, Thermo Fisher Scientific), TRPV2 siRNA (Mission siRNA, Mm_Trpv2_6139, Sigma), or the corresponding negative control siRNAs (Negative Control No. 1 for Silencer Select siRNA, SIC-001 for Mission siRNA, respectively) using Lipofectamine 2000 Transfection Reagent according to the manufacturer's protocol. Ca^{2+} imaging experiments were performed 24 h after transfection.

To examine knockdown efficiency, total RNA from siRNA-treated cells was isolated, and mRNA expression levels were monitored using RT-PCR as described above. PCR was terminated during the linear amplification phase for each product. Products were electrophoresed in 2% agarose gels containing 1 mg/liter ethidium bromide. Images were analyzed using ImageJ (National Institutes of Health, Bethesda, MD), and the fluorescence intensity of each band was quantified.

Ca^{2+} imaging

GLUTag cells plated on coverslips for 2 days were loaded with 250 nM Fluo-4 AM (Dojindo, Kumamoto, Japan) in modified Ringer Buffer (RB: 140 mM NaCl, 3.5 mM KCl, 0.5 mM NaH_2PO_4, 0.5 mM $MgSO_4$, 1.5 mM $CaCl_2$, 10 mM HEPES, 2 mM $NaHCO_3$) containing 5 mM glucose. After incubation for 20 min at 37 °C under 5% CO_2, the cells were washed twice, added to RB containing 0.1 mM glucose, and mounted on a stage heated at 37 °C. Imaging was performed using an inverted microscope (IX-71, Olympus, Tokyo, Japan) equipped with an oil-immersion objective lens (UApo/340, 40×, NA = 1.35, Olympus) and an EM-CCD camera (Evolve, Photometrics, Tucson, AZ), whose exposure was controlled by MetaMorph software (Molecular Devices, Sunnyvale, CA). The cells were excited using a xenon lamp, and images were acquired every 5 s

for 20 min. LPI stimulation was performed with a pipette 180 s after the initiation of image acquisition.

Total internal reflection fluorescence microscopy

GLUTag cells transfected with Lifeact-EGFP or TRPV2-EGFP were washed and imaged as described above. Imaging was performed using an inverted microscope (ECLIPSE Ti-E, Nikon, Tokyo, Japan). We used a high numerical aperture objective lens (CFI Apochromat TIRF, 100×, NA = 1.49, Nikon), and incident light for total internal reflection illumination was introduced from the objective lens through a single-mode optical fiber and two illumination lenses (TI-TIRF, Nikon). An optically pumped semiconductor 488-nm laser (Sapphire 488LP, 30 milliwatts, Coherent, Santa Clara, Canada) was used through a band-pass filter (HQ535/30m, Chroma, Bellows Falls, VT) as an emission filter. The laser beam was passed through an electromagnetically driven shutter (TI-TIRF, Nikon), and the shutter was opened synchronously with an EM-CCD camera (iXon, Andor, Belfast, UK) whose exposure was controlled by MetaMorph software. Images were acquired every 500 ms for 20 min.

Enzyme-linked immunosorbent assay

GLUTag cells were plated in 6-well plates at 2.5–5 × 10^5 cells per well. RNA interference was performed as described above. Two days after plating cells were washed twice with RB containing 5 mM glucose for 10 min at 37 °C under 5% CO_2. Then either vehicle solution (dimethyl sulfoxide), LPI, or LPI plus inhibitors in RB containing 0.1 mM glucose were applied to the cells and incubated for 30 min at 37 °C under 5% CO_2. After centrifugation at 1000 × *g* for 10 min at 4 °C, supernatant was used for analysis with the Glucagon-Like Peptide-1 (Active) ELISA kit (Merck Millipore) and microplate reader (Mithras LB 940, Berthold, Bad Wildbad, Germany).

Acute preparation of primary cultured mouse small intestinal cells

All experiments with animals were performed in accordance with the ethical guidelines for animal care and use of the University of Tokyo. In each experiment, three C57BL/6J mice (SLC, Shizuoka, Japan) at 8 weeks old were sacrificed by cervical dislocation after free access to water and food overnight. Small intestines were collected and cut into small pieces in ice-cold PBS. After centrifugation of 100 × g for 5 min at 4 °C, supernatant was removed, and the precipitant was minced in 10 ml of ice-cold PBS for 3 min. Then the mixture was centrifuged at 100 × *g* for 5 min at 4 °C, supernatant was removed, and the precipitant was suspended in 18 ml of RB. 500 μl of suspended samples were plated in 24-well plates and stimulated with either vehicle solution (dimethyl sulfoxide), LPI, or Fsk + IBMX with DPP IV inhibitor (Merck Millipore) for 1 h at 37 °C under 5% CO_2. Samples were centrifuged at 1000 × *g* for 10 min at 4 °C, and the supernatant was used for enzyme-linked immunosorbent assay. Data were normalized with tissue weight as pM/mg.

Imaging data analysis

Images acquired from live cell imaging experiments were analyzed using both ImageJ and MetaMorph software. Basal fluorescence intensity, normalized to 100%, was calculated as the average fluorescence intensity between 150 and 180 s from the beginning of image acquisition. To calculate the area under the curve, a photobleach curve was plotted as a single exponential curve between 185 and 1200 s, 245 and 1200 s (in + *RR* of Fig. 4*C*), or 365 and 1200 s (in Fig. 6*B*). The area between the photobleach curve and the acquired time course was used for statistical analysis.

To determine the density of focal adhesions, we counted the number of Lifeact-EGFP-derived fluorescent dots (Fig. 3*C*) using ImageJ. In brief, images were binarized with "subtract background" and "threshold," and fluorescent dots were defined as regions between 4 and 32 $pixel^2$ and circularity between 0.5 and 1.0 in "analyze particles." The number of these dots was divided by the area of each cell.

For statistical analysis, data are shown as the mean ± S.D. Means were compared by either Welch's *t* test or one-way ANOVA followed by Tukey's or Dunnett's post hoc test using GraphPad Prism 6 software (GraphPad software, La Jolla, CA).

Author contributions—K. H., Te. K., K. H. A., and Ta. K. performed the experiments and the data analysis. K. H., Te. K., K. N., K. O., and T. T. designed the study and wrote the manuscript.

Acknowledgments—We thank Drs. Roland Wedlich-Soldner and Daniel Drucker for kindly providing Lifeact-EGFP plasmid and GLUTag cells, respectively.

References

1. Flint, A., Raben, A., Astrup, A., and Holst, J. J. (1998) Glucagon-like peptide 1 promotes satiety and suppresses energy intake in humans. *J. Clin. Invest.* **101,** 515–520
2. Xu, G., Stoffers, D. A., Habener, J. F., and Bonner-Weir, S. (1999) Exendin-4 stimulates both beta-cell replication and neogenesis, resulting in increased beta-cell mass and improved glucose tolerance in diabetic rats. *Diabetes* **48,** 2270–2276
3. Ezcurra, M., Reimann, F., Gribble, F. M., and Emery, E. (2013) Molecular mechanisms of incretin hormone secretion. *Curr. Opin. Pharmacol.* **13,** 922–927
4. Reimann, F., Williams, L., da Silva Xavier, G., Rutter, G. A., and Gribble, F. M. (2004) Glutamine potently stimulates glucagon-like peptide-1 secretion from GLUTag cells. *Diabetologia* **47,** 1592–1601
5. Reimann, F., Habib, A. M., Tolhurst, G., Parker, H. E., Rogers, G. J., and Gribble, F. M. (2008) Glucose sensing in L cells: a primary cell study. *Cell Metab.* **8,** 532–539
6. Oya, M., Kitaguchi, T., Pais, R., Reimann, F., Gribble, F., and Tsuboi, T. (2013) The G protein-coupled receptor family C group 6 subtype A (GPRC6A) receptor is involved in amino acid-induced glucagon-like peptide-1 secretion from GLUTag cells. *J. Biol. Chem.* **288,** 4513–4521
7. Xiong, Y., Swaminath, G., Cao, Q., Yang, L., Guo, Q., Salomonis, H., Lu, J., Houze, J. B., Dransfield, P. J., Wang, Y., Liu, J. J., Wong, S., Schwandner, R., Steger, F., Baribault, H., *et al.* (2013) Activation of FFA1 mediates GLP-1 secretion in mice: evidence for allosterism at FFA1. *Mol. Cell. Endocrinol.* **369,** 119–129
8. Claustre, J., Brechet, S., Plaisancie, P., Chayvialle, J. A., and Cuber, J. C. (1999) Stimulatory effect of beta-adrenergic agonists on ileal L cell secretion and modulation by α-adrenergic activation. *J. Endocrinol.* **162,** 271–278
9. Ellingsgaard, H., Hauselmann, I., Schuler, B., Habib, A. M., Baggio, L. L., Meier, D. T., Eppler, E., Bouzakri, K., Wueest, S., Muller, Y. D., Hansen, A. M., Reinecke, M., Konrad, D., Gassmann, M., Reimann, F., *et al.* (2011) Interleukin-6 enhances insulin secretion by increasing glucagon-like peptide-1 secretion from L cells and alpha cells. *Nat. Med.* **17,** 1481–1489

10. Harada, K., Kitaguchi, T., and Tsuboi, T. (2015) Integrative function of adrenaline receptors for glucagon-like peptide-1 exocytosis in enteroendocrine L cell line GLUTag. *Biochem. Biophys. Res. Commun.* **460,** 1053–1058
11. Makide, K., Uwamizu, A., Shinjo, Y., Ishiguro, J., Okutani, M., Inoue, A., and Aoki, J. (2014) Novel lysophosphoplipid receptors: their structure and function. *J. Lipid Res.* **55,** 1986–1995
12. Ishii, I., Fukushima, N., Ye, X., and Chun, J. (2004) Lysophospholipid receptors: signaling and biology. *Annu. Rev. Biochem.* **73,** 321–354
13. Metz, S. A. (1986) Lysophosphatidylinositol, but not lysophosphatidic acid, stimulates insulin release. A possible role for phospholipase A2 but not *de novo* synthesis of lysophospholipid in pancreatic islet function. *Biochem. Biophys. Res. Commun.* **138,** 720–727
14. Metz, S. A. (1988) Mobilization of cellular Ca^{2+} by lysophospholipids in rat islets of langerhans. *Biochim. Biophys. Acta* **968,** 239–252
15. Pan, C. Y., Wu, A. Z., and Chen, Y. T. (2007) Lysophospholipids regulate excitability and exocytosis in cultured bovine chromaffin cells. *J. Neurochem.* **102,** 944–956
16. Monet, M., Gkika, D., Lehen'kyi, V., Pourtier, A., Vanden Abeele, F., Bidaux, G., Juvin, V., Rassendren, F., Humez, S., and Prevarsakaya, N. (2009) Lysophospholipids stimulate prostate cancer cell migration via TRPV2 channel activation. *Biochim. Biophys. Acta* **1793,** 528–539
17. Bondarenko, A. I., Malli, R., and Graier, W. F. (2011) The GPR55 agonist lysophosphatidylinositol directly activates intermediate-conductance Ca^{2+}-activated K^+ channels. *Pflugers Arch.* **462,** 245–255
18. AlSuleimani, Y. M., and Hiley, C. R. (2015) The GPR55 agonist lysophosphatidylinositol relaxes rat mesenteric resistance artery and induces Ca^{2+} release in rat mesenteric artery endothelial cells. *Br. J. Pharmacol.* **172,** 3043–3057
19. Ma, M. T., Yeo, J. F., Farooqui, A. A., Zhang, J., Chen, P., and Ong, W. Y. (2010) Differential effects of lysophospholipids on exocytosis in rat PC12 cells. *J. Neural Transm.* **117,** 301–308
20. Oka, S., Nakajima, K., Yamashita, A., Kishimoto, S., and Sugiura, T. (2007) Identification of GPR55 as a lysophosphatidylinositol receptor. *Biochem. Biophys. Res. Commun.* **362,** 928–934
21. Ryberg, E., Larsson, N., Sjögren, S., Hjorth, S., Hermansson, N. O., Leonova, J., Elebring, T., Nilsson, K., Drmota, T., and Greasley, P. J. (2007) The orphan receptor GPR55 is a novel cannabinoid receptor. *Br. J. Pharmacol.* **152,** 1092–1101
22. Lauckner, J. E., Jensen, J. B., Chen, H. Y., Lu, H. C., Hille, B., and Mackie, K. (2008) GPR55 is a cannabinoid receptor that increases intracellular calcium and inhibits M current. *Proc. Natl. Acad. Sci. U.S.A.* **105,** 2699–2704
23. Henstridge, C. M., Balenga, N. A., Ford, L. A., Ross, R. A., Waldhoer, M., and Irving, A. J. (2009) The GPR55 ligand L-α-lysophosphatidylinositol promotes RhoA-dependent Ca^{2+} signaling and NFAT activation. *FASEB J.* **23,** 183–193
24. Henstridge, C. M., Balenga, N. A., Schröder, R., Kargl, J. K., Platzer, W., Martini, L., Arthur, S., Penman, J., Whistler, J. L., Kostenis, E., Waldhoer, M., and Irving, A. J. (2010) GPR55 ligands promote receptor coupling to multiple signalling pathways. *Br. J. Pharmacol.* **160,** 604–614
25. Waldeck-Weiermair, M., Zoratti, C., Osibow, K., Balenga, N., Goessnitzer, E., Waldhoer, M., Malli, R., and Graier, W. F. (2008) Integrin clustering enables anandamide-induced Ca^{2+} signaling in endothelial cells via GPR55 by protection against CB1-receptor-triggered repression. *J. Cell Sci.* **121,** 1704–1717
26. Bondarenko, A., Waldeck-Weiermair, M., Naghdi, S., Poteser, M., Malli, R., and Graier, W. F. (2010) GPR55-dependent and-independent ion signalling in response to lysophosphatidylinositol in endothelial cells. *Br. J. Pharmacol.* **161,** 308–320
27. Romero-Zerbo, S. Y., Rafacho, A., Díaz-Arteaga, A., Suárez, J., Quesada, I., Imbernon, M., Ross, R. A., Dieguez, C., Rodríguez de Fonseca, F., Nogueiras, R., Nadal, A., and Bermúdez-Silva, F. J. (2011) A role for the putative cannabinoid receptor GPR55 in the islets of Langerhans. *J. Endocrinol.* **211,** 177–185
28. McKillop, A. M., Moran, B. M., Abdel-Wahab, Y. H., and Flatt, P. R. (2013) Evaluation of the insulin releasing and antihyperglycaemic activities of GPR55 lipid agonists using clonal beta-cells, isolated pancreatic islets and mice. *Br. J. Pharmacol.* **170,** 978–990
29. Moreno-Navarrete, J. M., Catalán, V., Whyte, L., Díaz-Arteaga, A., Vázquez-Martínez, R., Rotellar, F., Guzmán, R., Gómez-Ambrosi, J., Pulido, M. R., Russell, W. R., Imbernón, M., Ross, R. A., Malagón, M. M., Dieguez, C., Fernández-Real, J. M., Frühbeck, G., and Nogueiras, R. (2012) The L-α-lysophosphatidylinositol/GPR55 system and its potential role in human obesity. *Diabetes* **61,** 281–291
30. Imbernon, M., Whyte, L., Diaz-Arteaga, A., Russell, W. R., Moreno, N. R., Vazquez, M. J., Gonzalez, C. R., Díaz-Ruiz, A., Lopez, M., Malagón, M. M., Ross, R. A., Dieguez, C., and Nogueiras, R. (2014) Regulation of GPR55 in rat white adipose tissue and serum LPI by nutritional status, gestation, gender, and pituitary factors. *Mol. Cell. Endocrinol.* **383,** 159–169
31. Riedl, J., Crevenna, A. H., Kessenbrock, K., Yu, J. H., Neukirchen, D., Bista, M., Bradke, F., Jenne, D., Holak, T. A., Werb, Z., Sixt, M., and Wedlich-Soldner, R. (2008) Lifeact: a versatile marker to visualize F-actin. *Nat. Methods* **5,** 605–607
32. Kiuchi, T., Higuchi, M., Takamura, A., Maruoka, M., and Watanabe, N. (2015) Multitarget super-resolution microscopy with high-density labeling by exchangeable probes. *Nat. Methods* **12,** 743–746
33. Kuipers, D., Mehonic, A., Kajita, M., Peter, L., Fujita, Y., Duke, T., Charras, G., and Gale, J. E. (2014) Epithelial repair is a two-stage process driven first by dying cells and then by their neighbours. *J. Cell Sci.* **127,** 1229–1241
34. Vriens, J., Appendino, G., and Nilius, B. (2009) Pharmacology of vanilloid transient receptor potential cation channels. *Mol. Pharmacol.* **75,** 1262–1279
35. Gettys, T. W., Ramkumar, V., Surwit, R. S., and Taylor, I. L. (1995) Tissue-specific alterations in G protein expression in genetic versus diet-induced models of non-insulin-dependent diabetes mellitus in the mouse. *Metabolism* **44,** 771–778
36. Matsuda, N., Hattori, Y., Gando, S., Watanuki, S., Kemmotsu, O., and Kanno, M. (2000) Differential gene transcriptional regulation of G_i isoforms and G_s protein expression in diabetic rat hearts. *Naunyn. Schmiedebergs. Arch. Pharmacol.* **361,** 53–60
37. Martin, N. P., Whalen, E. J., Zamah, M. A., Pierce, K. L., and Lefkowitz, R. J. (2004) PKA-mediated phosphorylation of the β_1-adrenergic receptor promotes G_s/G_i switching. *Cell Signal.* **16,** 1397–1403
38. Cruciani, R. A., Dvorkin, B., Morris, S. A., Crain, S. M., and Makman, M. H. (1993) Direct coupling of opioid receptors to both stimulatory and inhibitory guanine nucleotide-binding proteins in F-11 neuroblastoma-sensory neuron hybrid cells. *Proc. Natl. Acad. Sci. U.S.A.* **90,** 3019–3023
39. Lawler, O. A., Miggin, S. M., and Kinsella, B. T. (2001) Protein kinase A-mediated phosphorylation of serine 357 of the mouse prostacyclin receptor regulates its coupling to G_s-, to G_i-, and to G_q-coupled effector signaling. *J. Biol. Chem.* **276,** 33596–33607
40. Hou, J. C., Shigematsu, S., Crawford, H. C., Anastasiadis, P. Z., and Pessin, J. E. (2006) Dual regulation of Rho and Rac by p120 catenin controls adipocyte plasma membrane trafficking. *J. Biol. Chem.* **281,** 23307–23312
41. Chun, K. H., Araki, K., Jee, Y., Lee, D. H., Oh, B. C., Huang, H., Park, K. S., Lee, S. W., Zabolotny, J. M., and Kim, Y. B. (2012) Regulation of glucose transport by ROCK1 differs from that of ROCK2 and is controlled by actin polymerization. *Endocrinology* **153,** 1649–1662
42. Tsuchiya, A., Kanno, T., Shimizu, T., Tanaka, A., and Nishizaki, T. (2015) Rac1 and ROCK are implicated in the cell surface delivery of GLUT4 under the control of the insulin signal mimetic diDCP-LA-PE. *J. Pharmacol. Sci.* **128,** 179–184
43. Nagasawa, M., and Kojima, I. (2012) Translocation of calcium-permeable TRPV2 channel to the podosome: Its role in the regulation of podosome assembly. *Cell Calcium* **51,** 186–193
44. Porat-Shliom, N., Milberg, O., Masedunskas, A., and Weigert, R. (2013) Multiple roles for the actn cytoskeleton during regulated exocytosis. *Cell. Mol. Life Sci.* **70,** 2099–2121
45. Rudolf, R., Kögel, T., Kuznetsov, S. A., Salm, T., Schlicker, O., Hellwig, A., Hammer, J. A., 3rd, and Gerdes, H. H. (2003) Myosin Va facilitates the distribution of secretory granules in the F-actin rich cortex of PC12 cells. *J. Cell Sci.* **116,** 1339–1348

46. Nieto-Posadas, A., Picazo-Juárez, G., Llorente, I., Jara-Oseguera, A., Morales-Lázaro, S., Escalante-Alcalde, D., Islas, L. D., and Rosenbaum, T. (2011) Lysophosphatidic acid directly activates TRPV1 through a C-terminal binding site. *Nat. Chem. Biol.* **8,** 78–85
47. Andersson, D. A., Nash, M., and Bevan, S. (2007) Modulation of the cold-activated channel TRPM8 by lysophospholipids and polyunsaturated fatty acids. *J. Neurosci.* **27,** 3347–3355
48. Vanden Abeele, F., Zholos, A., Bidaux, G., Shuba, Y., Thebault, S., Beck, B., Flourakis, M., Panchin, Y., Skryma, R., and Prevarskaya, N. (2006) Ca^{2+}-independent phospholipase A2-dependent gating of TRPM8 by lysophospholipids. *J. Biol. Chem.* **281,** 40174–40182
49. Meadows, A., Lee, J. H., Wu, C. S., Wei, Q., Pradhan, G., Yafi, M., Lu, H. C., and Sun, Y. (2015) Deletion of G-protein-coupled receptor 55 promotes obesity by reducing physical activity. *Int. J. Obes.* (*Lond*) **40,** 417–424